THE JOURNAL OF BIOLOGICAL CHEMISTRY VOL. 291, NO. 35, pp. 18419–18429, August 26, 2016

Enzymatically Inactive Procaspase 1 stabilizes the ASC Pyroptosome and Supports Pyroptosome Spreading during Cell Division*[S]

Received for publication, February 1, 2016, and in revised form, June 30, 2016 Published, JBC Papers in Press, July 8, 2016, DOI 10.1074/jbc.M116.718668

Robert Stein[‡], Franz Kapplusch[‡], Michael Christian Heymann[‡], Susanne Russ[‡], Wolfgang Staroske[§], Christian Michael Hedrich[‡], Angela Rösen-Wolff[‡], and Sigrun Ruth Hofmann[‡1]

From the [‡]Department of Pediatrics, Medizinische Fakultät Carl Gustav Carus, and [§]Biotechnology Center, Technische Universität Dresden, 01307 Dresden, Germany

Caspase-1 is a key player during the initiation of pro-inflammatory innate immune responses, activating pro-IL-1β in so-called inflammasomes. A subset of patients with recurrent febrile episodes and systemic inflammation of unknown origin harbor mutations in *CASP1* encoding caspase-1. *CASP1* variants result in reduced enzymatic activity of caspase-1 and impaired IL-1β secretion. The apparent paradox of reduced IL-1β secretion but systemic inflammation led to the hypothesis that *CASP1* mutations may result in variable protein interaction clusters, thus activating alternative signaling pathways. To test this hypothesis, we established and characterized an *in vitro* system of transduced immortalized murine macrophages expressing either WT or enzymatically inactive (p.C284A) procaspase-1 fusion reporter proteins. Macrophages with variant p.C284A caspase-1 did not secrete IL-1β and exhibited reduced inflammatory cell death, referred to as pyroptosis. Caspase-1 and apoptosis-associated speck-like protein containing a CARD (ASC) formed cytosolic macromolecular complexes (so-called pyroptosomes) that were significantly increased in number and size in cells carrying the p.C284A caspase-1 variant compared with WT caspase-1. Furthermore, enzymatically inactive caspase-1 interacted with ASC longer and with increased intensity compared with WT caspase-1. Applying live cell imaging, we documented for the first time that pyroptosomes containing enzymatically inactive variant p.C284A caspase-1 spread during cell division. In conclusion, variant p.C284A caspase-1 stabilizes pyroptosome formation, potentially enhancing inflammation by two IL-1β-independent mechanisms: pyroptosomes convey an enhanced inflammatory stimulus through the recruitment of additional proteins (such as RIP2, receptor interacting protein kinase 2), which is further amplified through pyroptosome and cell division.

Caspase-1 is a key player during innate immune responses. It aids to control pathogens and danger signals by triggering pyroptotic cell death. Together with caspase-11 and -12 in mice and caspase-4, -5, and -12 in humans, caspase-1 belongs to the family of inflammatory caspases, which are produced as inactive forms. After the detection of pathogens or cytoplasmic danger signals, inactive caspase-1 monomers recruit to multiprotein complexes referred to as inflammasomes (1–3). In such inflammasomes, inactive procaspases are autoprocessed into caspase activation and recruitment domains (CARDs),[2] the p10 and the p20 subunits (4). Two p10 and two p20 proteins subsequently form the active caspase-1 tetramer, which then cleaves and thereby activates IL-1β in the so-called canonical inflammasome pathway (5, 6). Furthermore, inflammatory caspases induce pro-inflammatory cell death, referred to as pyroptosis, which involves cell swelling, cell lysis, and the release of cytoplasmic contents (7, 8). Pyroptosis depends on the activation of caspase-4, -5, or -11 and caspase-1 (9–11). Caspase-1 or -11 cleaves gasdermin D, a gasdermin domain-containing protein, at amino acid aspartate 276. The resulting N-terminal amino residue is responsible for the induction of pyroptosis (10, 11).

Recently, naturally occurring genetic variants of the *CASP1* gene were associated with recurrent fevers and systemic inflammation in individuals with "interleukin 1-converting enzyme fever" (12, 13). Caspase-1 variants exhibit reduced or absent enzymatic activity, resulting in impaired autoprocessing of inactive procaspase-1 and, subsequently, reduced cleavage, activation, and release of the pro-inflammatory cytokine IL-1β. Thus, systemic inflammation in these patients most likely results from the induction of alternative pro-inflammatory pathways. Indeed, enzymatically inactive procaspase-1 variants were documented to maintain prolonged interactions with receptor-interacting protein kinase 2 (RIP2) through its CARD, which results in enhanced NF-κB activation, resembling an alternative pro-inflammatory pathway (14).

Canonical inflammasome activation comprises the assembly of multiprotein complexes containing sensor molecules, including cytosolic pattern recognition receptors from the NOD-like receptor (NLR) family, pyrin and HIN domain-containing protein family, the adaptor molecule apoptosis-associated speck-like protein containing a CARD (ASC),

* This work was supported by German Research Foundation (DFG) Grants KFO249, TP2, HO4510/1–2 (to S. R. H.) and TP1 and RO/471–11 (to A. R. W.) and the Else Kröner Fresenius Stiftung (Else-Kröner-Promotionskolleg, EKFS Foundation) (to R. S.). The authors declare that they have no conflicts of interest with the contents of this article.

[S] This article contains supplemental Movies 1–5.

[1] To whom correspondence should be addressed: Dept. of Pediatrics, University Hospital Carl Gustav Carus, Fetscherstr. 74, 01307 Dresden, Germany. Tel.: 49-351-458-6883; Fax: 49-351-458-4381; E-mail: sigrun.hofmann@uniklinikum-dresden.de.

[2] The abbreviations used are: CARD, caspase activation and recruitment domain; NLR, NOD-like receptor; ASC, apoptosis-associated speck-like protein containing a caspase activation and recruitment domain; iBMDM, immortalized bone marrow-derived macrophages; NA, numerical aperture; EX, excitation; EM, emission; Ch, mCherry.

and the effector molecule procaspase-1. The NLR family pyrin domain-containing 3 (NLRP3) inflammasome, which responds to recognition of pathogen- or damage-associated molecular patterns such as nigericin, ATP, urate, and cholesterol crystals, is the most intensively studied (15–18). During inflammasome assembly, ASC rapidly oligomerizes around NLRP3 molecules, forming filamentous structures that assemble into large protein aggregates or specks (so-called pyroptosomes) that localize to the perinuclear region of the cell (19, 20). ASC specks serve as activation platforms, recruiting and activating caspase-1 through multimerization and autoproteolysis. Recent studies demonstrated that self-organization of pyrin domains, NLRs, or PYHIN family proteins result in the assembly of helical ASC: pyrin domain filaments that subsequently promote the formation of caspase-1 filaments (20, 21). In response to ASC speck formation, activated cells undergo pyroptosis, by which intracellularly assembled ASC specks are released to the extracellular space. Of note, released ASC specks remain active, resulting in the activation and processing of procaspase-1 and pro-IL-1β in the extracellular compartment (22, 23). Furthermore, extracellular specks are internalized by phagocytes such as macrophages, promoting inflammasome activation in those cells. Thus, speck internalization amplifies inflammatory responses through a recently identified form of cell-to-cell communication (22, 23). Extracellular ASC specks can be detected in fluids and tissues from patients with chronic inflammatory lung disease and cryopyrin-associated periodic syndrome but not in body fluids from patients with other autoinflammatory syndromes (22).

In this study, we aimed to investigate whether the alteration of speck formation or pyroptosis by the enzymatically inactive variant p.C284A caspase-1 may resemble another, previously not appreciated pathophysiological mechanism in patients suffering from autoinflammatory disease. We demonstrate that the enzymatically inactive p.C284A variant forms larger specks (pyroptosomes) in the cytosol and maintains extended and more intense interactions with ASC compared with wild-type caspase-1. Applying live cell imaging, we determined for the first time that pyroptosomes of enzymatically inactive procaspase-1 spread during cell division. Thus, we conclude that variant p.C284A caspase-1 stabilizes pyroptosome formation, subsequently enhancing inflammation through increased recruitment and prolonged interaction with further pro-inflammatory proteins (*e.g.* RIP2) and the amplification of pyroptosome stimuli through spreading during cell division.

Results

Transduction of Immortalized Murine Macrophages with Lentiviral Constructs Encoding Fluorophore-tagged Procaspase-1 Allows for Induction of Caspase-1 Activation, Speck Formation, and Inflammatory Cell Death—To investigate potential differences in protein interactions and subcellular distribution of variant caspase-1 in living cells, we established an *in vitro* cell system using fluorophore-tagged proteins. WT or enzymatically inactive caspase-1 carrying a missense mutation in its active center (p.C284A) were N-terminally fused to the red fluorescent protein mCherry (Fig. 1*A*) and introduced into immortalized caspase-1/11 knockout macrophages (iBMDM$^{casp1/11\text{-}ko}$) by retroviral transduction. The transduction efficiency was tested by fluorescence-based flow cytometry analysis (data not shown), and Western blotting showed comparable protein expression levels between cell lines (Fig. 1*B*). The functionality of our cell model was evaluated by mimicking bacterial infection with ultrapure LPS as a priming step (24) and nigericin as an NLRP3-specific activator of caspase-1 (25). IL-1β secretion was used as a readout for caspase-1 activity (Fig. 1*C*). Only cells expressing mCherry that was N-terminally fused to WT caspase-1 (Ch-WT) secreted mature IL-1β when treated with both LPS and nigericin. Consistent with these observations, we were able to detect p10 subunit release of the active caspase-1 tetramer only in the supernatant of cells challenged under the same conditions (Fig. 1*B*). Furthermore, only the addition of both LPS and nigericin resulted in a significant increase of lactate dehydrogenase release into supernatants of Ch-WT-transduced cells, which was used as a measure of cell death (Fig. 1*D*). In contrast, cells expressing mCherry N-terminally fused to variant p.C284A caspase-1 (Ch-C284A) did neither secrete mature IL-1β nor release increased amounts of lactate dehydrogenase into their supernatants (Fig. 1, *B–D*). Hence, assuming that our method was sufficiently reproducing physiological macrophage functions *in vitro* and was not affected by the fluorescent tags, we conducted live cell imaging experiments under the aforementioned conditions (26). In response to stimulation with LPS or nigericin alone, cells did not show remarkable changes. However, Ch-WT and Ch-C284A cells formed one cytosolic macromolecular speck ~20 min after the addition of nigericin when a priming step with LPS had preceded (supplemental Movie 1 and Fig. 1*F*). Within 5 min after speck formation, Ch-WT cells started to swell and lose membrane integrity by vesicle formation, whereas the Ch-WT speck slowly faded (supplemental Movie 1 and Fig. 2*A*). Cellular swelling and loss of membrane integrity resemble pro-inflammatory cell death, which is associated with IL-1β secretion, referred to as pyroptosis (7). Assuming that fading mCherry-signals in specks are the consequence of caspase-1 autoprocessing, leading to the separation of mCherry-labeled CARD and unlabeled p20/p10 (Fig. 1*A*), we wondered about the dynamics and distribution of molecule domains not directly fused to mCherry. We stained stimulated iBMDM$^{casp1/11\text{-}ko}$ cells with an antibody targeting the p10 subunit of caspase-1 and found all p10 specks co-localizing with Ch-WT specks (data not shown). Thus, we concluded that the mCherry signal represents the localization of the entire procaspase-1 molecule within the speck.

Enzymatically Inactive Caspase-1 Enhances Speck Formation and Prevents Macrophages from Undergoing Pyroptosis—Performing the aforementioned stimulation assays with LPS and nigericin in iBMDM$^{casp1/11\text{-}ko}$ that expressed the variant p.C284A caspase-1, we failed to detect mature IL-1β, cleavage products of caspase-1, or increased lactate dehydrogenase release to the supernatant. This indicates that the p.C284A variant is unable to convey autoprocessing of caspase-1, IL-1β activation, and pyroptosis (Fig. 1, *B–D*). Of note, cells were still capable of assembling Ch-C284A specks (Fig. 1, *E* and *F*). Variant caspase-1 macrophages even exhibited significantly increased numbers of specks compared with WT cells (Fig. 1*E*).

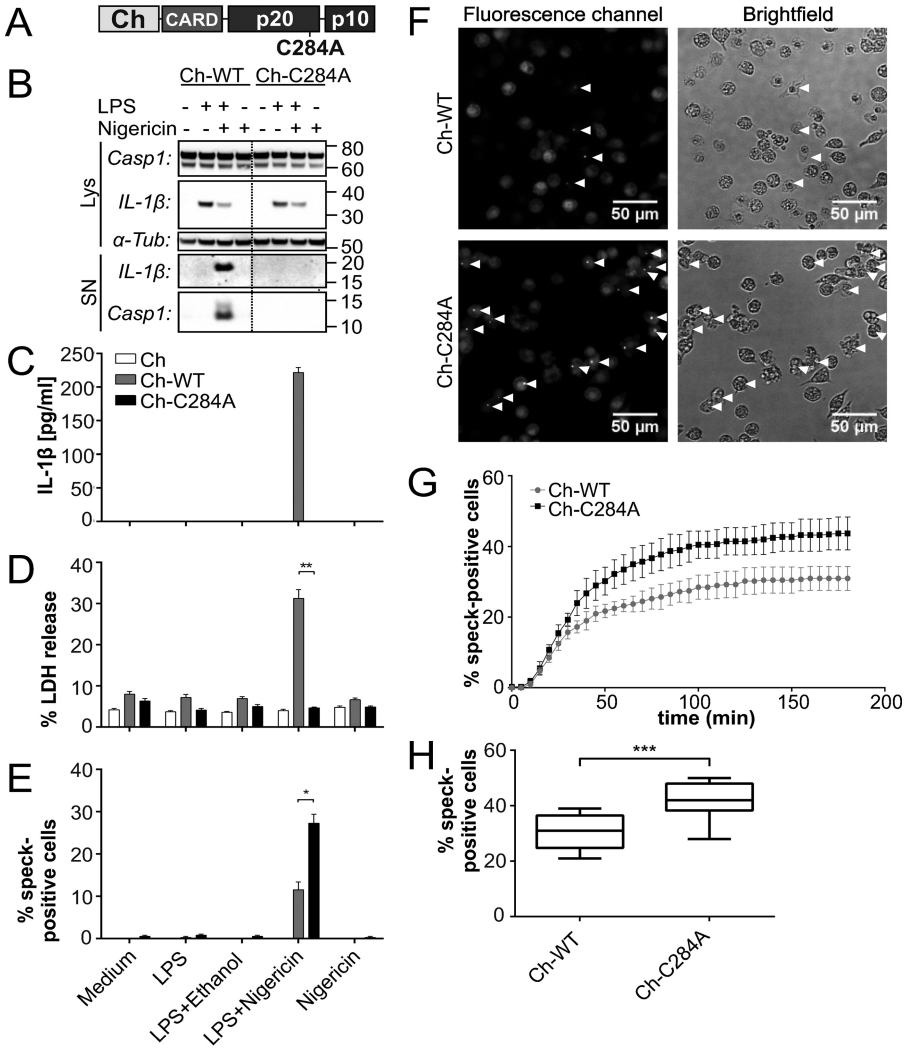

FIGURE 1. **Enzymatically inactive caspase-1 prevents macrophages from pyroptosis but not from speck formation.** Fusion proteins of the red fluorophore mCherry tagged to either WT caspase-1 (Ch-WT) or enzymatic inactive caspase-1 (Ch-C284A) were expressed in immortalized bone-marrow-derived caspase-1/11-knock-out macrophages (iBMDM$^{casp1/11\text{-}ko}$). mCherry alone served as control. Caspase-1 activation was induced by priming with 5 μg/ml LPS for 3 h, followed by 10 μM nigericin for 1 h (*B–E*) or 3 h, respectively (*F–H*). *A*, the red fluorescent protein mCherry (Ch) was fused to the N-terminal CARD of procaspase-1. In response to activation, the pro-enzyme is cleaved into the CARD and the active p20 and p10 subunits. *B*, by Western blotting, we detected intracellular protein levels (*Lys*) of the procaspase-1 fusion protein (*Casp1*, 74 kDa), partially degraded caspase-1 (60 kDa), and pro-interleukin-1β (*IL-1β*, 33 kDa) as well as the active cleavage products in supernatants (*SN*; IL-1β, 17.5 kDa; Casp1, 12 kDa, referring to the p10 subunit). α-Tubulin (α-*Tub*) served as a loading control. *C*, IL-1β release into supernatants was measured by cytometric bead array ($n = 6$). *D*, lactate dehydrogenase (*LDH*) release into the supernatant represents cell death ($n = 6$). *E*, the number of Ch-WT or Ch-C284A specks that were observed by fluorescence microscopy were counted and related to the total amount of nuclei (Hoechst stains) within the same field ($n = 4$). *F*, representative microscopy images were acquired 3 h after the addition of nigericin. *Arrowheads* indicate cells that formed specks. *G*, at each time point (every 5 min), specks emerging for the first time were counted and added to the number of specks in previous slides. Results of four replicates from one experiment are provided, which are representative of three independent experiments. *H*, box plots indicate the cumulative number of specks after 3 h of nigericin treatment ($n = 12$ from three independent experiments). Statistical significance was determined using Mann-Whitney test. *, $p < 0.05$; **, $p < 0.01$; ***, $p < 0.001$.

We wondered whether Ch-WT specks had already vanished before they could be detected by microscopy, contributing to the observed differences in speck numbers. To test this possibility, we evaluated both cell lines for 3 h after NLRP3 stimulation in short intervals (every 5 min or every 7.2 min, respectively) and added the number of newly formed specks to the speck number of the previous slide at each time point, gaining a cumulative amount of specks (Fig. 1*G*). Still, the previously determined differences remained (Fig. 1*H*).

Attenuated Enzymatic Activity of Variant p.C284A Caspase-1 Stabilizes the ASC Pyroptosome—Pyroptosis was linked to the formation of macromolecular specks of oligomerized ASC molecules, termed the ASC pyroptosome (27). Thus, we introduced ASC and either Ch-WT or Ch-C284A into iBMDM$^{casp1/11\text{-}ko}$. ASC had been fused to enhanced GFP (EGFP) at its N terminus (GFP-ASC). Again, we detected comparable protein expression of caspase-1 and ASC by Western blotting and fluorescence-based flow cytometry analysis and confirmed the functional activity of caspase-1 by IL-1β and lactate dehydrogenase release into cell culture supernatants (data not shown). Caspase-1 specks co-localized with ASC specks in response to NLRP3 stimulation (Fig. 2*A*). Furthermore, both specks formed at the same time and followed the same dynamics (Fig. 2*A*). As before, macrophages expressing the enzymatically inactive variant p.C284A caspase-1 exhibited significantly higher cumulative numbers of specks 3 h after

addition of nigericin (comparable with Fig. 1, *F* and G; data not shown). Measuring speck intensities over time, we observed ASC and caspase-1 specks fading in Ch-WT cells immediately after their formation (Fig. 2, *B* and *C*). In contrast, specks remained stable and even increased in brightness within the first 20 min in Ch-C284A cells, although cytosolic fluorescence intensity levels before pyroptosome formation were slightly lower in Ch-WT cells (Fig. 2*B*, *−10.5 min time point*). Of note,

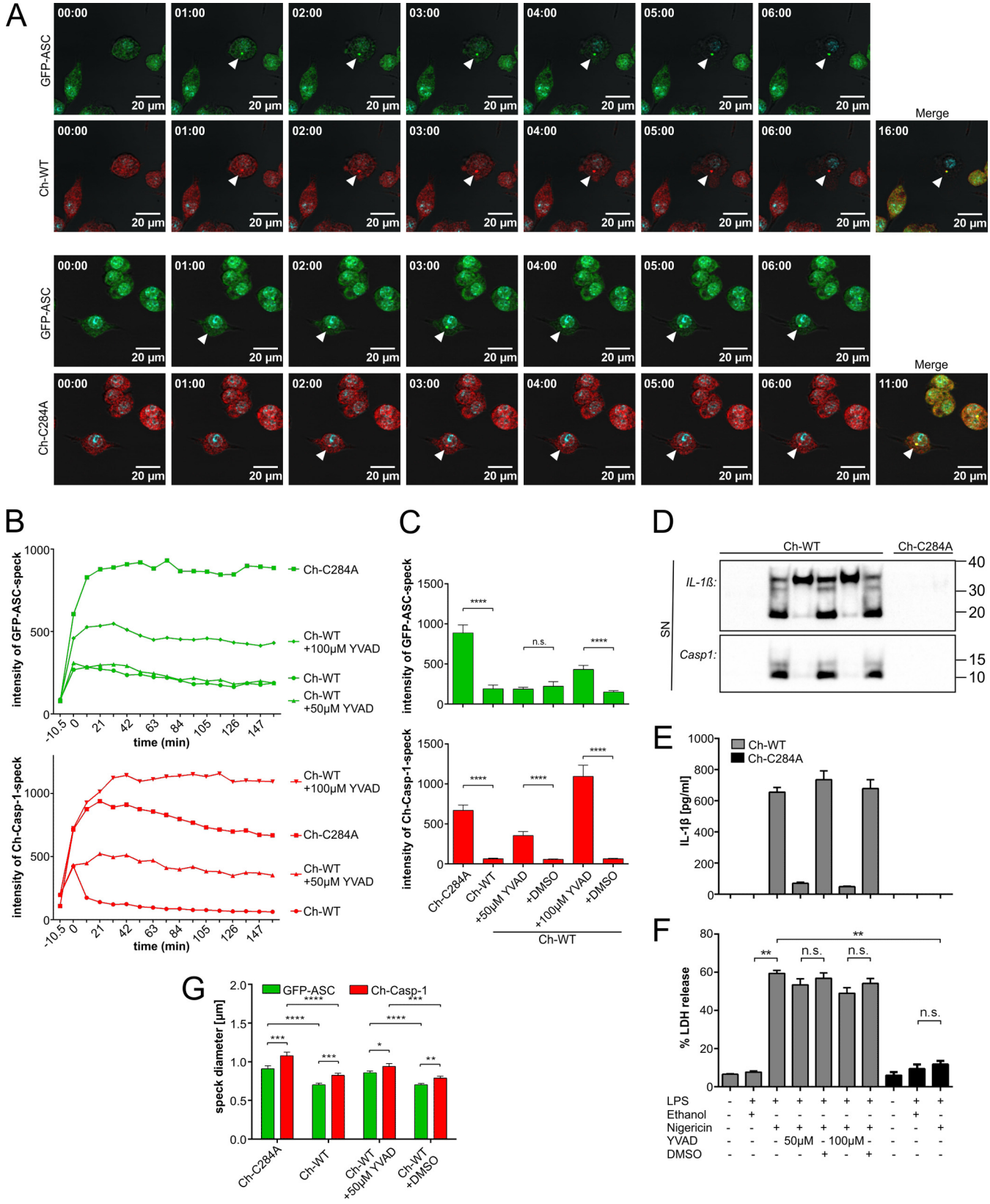

Ch-WT specks exhibited a more rapid decrease in fluorescence intensity compared with GFP-ASC within the same cell (Fig. 2*B*), suggesting caspase-1 autoprocessing as a possible explanation rather than loss of intracellular contents through pyroptosis. To further distinguish between cell death and autoprocessing as potential mechanisms for differences between fluorescence intensities, we added increasing amounts (50 and 100 μM) of the caspase-1 inhibitor Ac-YVAD-CMK to stimulated Ch-WT macrophages. Both concentrations were sufficient to nearly abrogate caspase-1 protease activity (Fig. 2, *D–F*). Surprisingly, although Ch-WT macrophages were not rescued from cell death (Fig. 2*F*), treatment with Ac-YVAD-CMK increased the fluorescence intensity of both GFP-ASC and Ch-WT specks in a dose-dependent manner. GFP-ASC specks, however, required higher inhibitor concentrations than Ch-WT specks (Fig. 2, *B* and *C*). We concluded that reduced enzymatic activity of caspase-1 stabilizes the pyroptosome independently of cell death.

Enzymatic Activity of Caspase-1 Influences the Size of ASC Pyroptosomes—Abrogating (Ch-C284A) or reducing (Ac-YVAD-CMK) the enzymatic activity of caspase-1 enlarged the size of the GFP-ASC and the mCherry-caspase-1 pyroptosome (Fig. 2*G*). We determined a mean ASC speck diameter of 0.7017 μm (S.D. $\pm$ 0.1267 μm) in Ch-WT cells, which was consistent with data from the literature (28), and a mean ASC speck diameter of 0.909 μm (S.D. $\pm$ 0.2223 μm) in Ch-C284A cells. Interestingly, the diameters of the caspase-1 specks were reproducibly larger than those of the ASC specks in all settings (Ch-WT mean speck diameter 0.8248 μm, S.D. $\pm$ 0.1467 μm; Ch-C284A mean speck diameter 1.0784 μm, S.D. $\pm$ 0.2643 μm).

Enzymatically Inactive Caspase-1 Interacts More with ASC—Given the observations mentioned above, we concluded that the increase in speck intensity and diameter may be the consequence of a larger number of ASC or procaspase-1 molecules assembling in the pyroptosome of Ch-C284A cells compared with Ch-WT cells. Thus, more molecules of variant p.C284A caspase-1 may interact with ASC in comparison with WT caspase-1. Indeed, more Ch-C284A molecules were co-immunoprecipitated with ASC in transduced iBMDM$^{casp1/11\text{-}ko}$ before and after NLRP3 stimulation (Fig. 3, *A* and *B*) compared with Ch-WT molecules. However, those results did not allow us to determine whether the observed protein interactions occurred within the pyroptosome or other cellular compartments. Also, increased numbers of caspase-1 molecules or a higher bonding affinity between interacting couples may be additional reasons for increased co-immunoprecipitation. Thus, we assessed protein interaction intensities between ASC and caspase-1 by measuring fluorescence resonance energy transfer applying fluorescence lifetime imaging microscopy (FLIM-FRET). This method is based on the assumption that the lifetime of an excited fluorescent donor (GFP-ASC) is quenched when it gets as close as 10 nm or less to an appropriate fluorescent acceptor (Ch-WT, Ch-C284A) (29). Within this radius, the donor transfers parts of its energy into the acceptor, which decreases the lifetime of the donor. Hence, a reduced lifetime indicates a small distance and thus close interaction between the donor and acceptor. Using a single-exponential decay model for data analysis, we detected increased interaction between procaspase-1 and ASC within Ch-C284A specks compared with Ch-WT specks (Fig. 3*C*). However, interacting and non-interacting molecules are always present at the same time, and both contribute to the FLIM signal. To further distinguish between those two components, we applied a double-exponential decay model. Cells with enzymatically inactive caspase-1 exhibited the highest fraction of FRET couples, representing the largest amount of molecules interacting with ASC (Fig. 3*D*). The lifetimes of FRET couples, indicating interaction strengths between each pair of molecules, were comparable between cell lines (Fig. 3*E*). We thus concluded that increased interactions between molecules in Ch-C284A cells were caused by a larger number of caspase-1 molecules oligomerizing in specks rather than a tighter bonding affinity of the mutant form.

Pyroptosomes Spread during Cell Division in Cells with Abrogated Caspase-1 Activity—The aforementioned experiments lasted for a maximum of 3 h after the induction of pyroptosome formation by addition of nigericin. At this time point, most of the macrophages bearing enzymatically inactive p.C284A caspase-1 were still alive. Thus, we wondered about speck persistence at later time points. Because nigericin caused toxic effects that were independent of pyroptosis (data not shown), we replaced cell culture supernatants after LPS priming and 1 h of nigericin treatment with fresh cell culture medium and performed live cell imaging on macrophages for up to 17 h. In agreement with our aforementioned observations, cells transduced with Ch-WT underwent pyroptosome formation and inflammatory cell death. Most of the macrophages carrying variant p.C284A caspase-1, however, remained viable and also started to proliferate again. Ch-C284A specks either remained unaltered, degenerated after several hours, or split up within

FIGURE 2. **Attenuated enzymatic activity of caspase-1 increases fluorescence intensity and size of the pyroptosome.** iBMDM$^{casp1/11\text{-}ko}$ cells expressed GFP-ASC in combination with either Ch-WT or Ch-C284A. Caspase-1 activation was induced by 3 h of priming with 5 μg/ml LPS, followed by 10 μM nigericin. Fluorescence life cell imaging was initiated subsequently. *A*, bright-field (*gray*) and Hoechst (*blue nuclei*) channels were merged with either the GFP channel (*green*, *first* and *third rows*), the cherry channel (*red*, *second* and *fourth rows*), or both (*Merge*). Representative images were chosen between 0–16 min (Ch-WT) or 0–11 min (Ch-C284A), respectively, after speck formation (*arrowheads*). *B* and *C*, cells expressing both fluorescent proteins were analyzed for speck formation. Graphs indicate mean values of maximum fluorescence intensities of Ch-WT or Ch-C284A specks (*red*) or GFP-ASC specks (*green*). First speck formation was set as the starting point (0 min) and assessed for each pyroptosome individually. Intensity levels 10.5 min before speck formation (*−10.5 min*) represent the background signal from the cytosol. DMSO as loading control was excluded from *E* for matters of clarity but included in *F*. Speck intensities after 158.5 min were chosen for statistical analysis in *F* ($n \geq 64$ of three independent experiments). *D–F*, cell lines (as labeled in *B* and *C*) were treated as indicated. Ethanol served as a loading control for nigericin and DMSO as a loading control for Ac-YVAD-CMK (*YVAD*). *D*, in Western blots from supernatants (*SN*), we detected the pro-form and active form of IL-1β (33 and 17.5 kDa, respectively) as well as the active caspase-1 p10 subunit (*Casp1*, 10 kDa). *E*, IL-1β release into supernatants was measured with cytometric bead arrays ($n = 2$). *F*, lactate dehydrogenase (*LDH*) release into supernatants represents cell death ($n = 6$). *G*, speck sizes were measured in cells expressing both mCherry-caspase-1 (*Ch-Casp-1*) and GFP-ASC ($n \geq 31$ of three independent experiments). Statistical significance was determined by Mann-Whitney test. *, $p < 0.05$; **, $p < 0.01$; ***, $p < 0.001$; ****, $p < 0.0001$; *n.s.*, not significant. Standard errors of the mean are indicated.

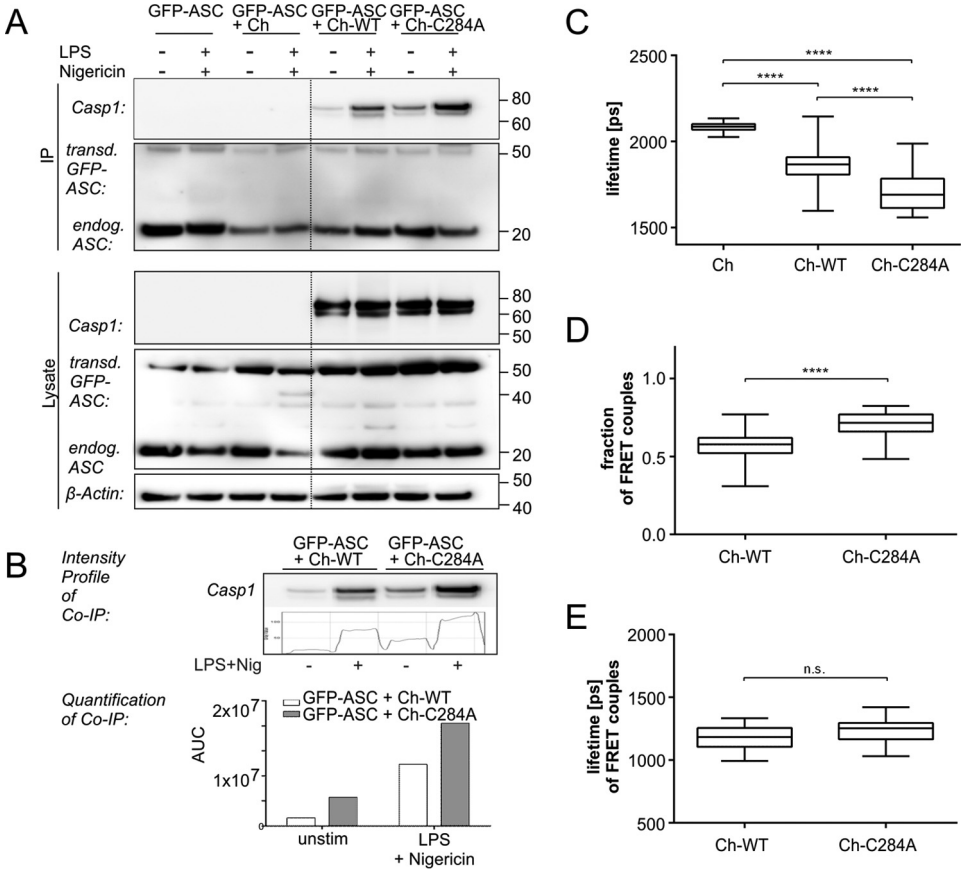

FIGURE 3. **Increased numbers of enzymatically inactive variant p.C284A caspase-1 molecules interact with ASC within pyroptosomes.** *A*, for co-immunoprecipitation (*IP*), iBMDM$^{casp1/11\text{-}ko}$ cells expressing GFP-ASC together with either Ch-WT or Ch-C284A were primed with LPS and then stimulated with nigericin as indicated. Cells were lysed and incubated with anti-ASC-coupled resins, followed by SDS-PAGE and Western blotting detection. More Ch-C284A molecules were co-immunoprecipitated with ASC in transduced iBMDM$^{casp1/11\text{-}ko}$ cells after NLRP3-stimulation (*first lane*) compared with Ch-WT molecules. *B*, densitometric analysis of co-immunoprecipitated proteins showed quantitatively the enhanced interaction between Ch-C284A molecules and ASC compared with Ch-WT molecules. *unstim*, unstimulated. *C–E*, iBMDM$^{casp1/11\text{-}ko}$ cells expressed GFP-ASC (donor) together with either Ch-WT or Ch-C284A (acceptor). mCherry served as a negative control. Caspase-1 activation was induced by 4 h of priming with 1 μg/ml LPS, followed by 10 μM nigericin. After 5 h, cells were fixed, and cells expressing both GFP-ASC and mCherry-caspase-1 (or mCherry alone) were analyzed by FLIM-FRET. *C*, first, data were fitted to single-exponential decay. Here a low lifetime indicated a short distance between donor and acceptor, hence, in our case, an overall close interaction. *D* and *E*, a double-exponential decay model allowed us to distinguish between interacting and non-interacting components contributing to the overall decay function. The fraction of FRET couples represents the amount of interacting donor-acceptor pairs. For example, a fraction of 1.0 would imply that every single GFP-ASC molecule found an mCherry-caspase-1 molecule with which to interact (*D*). The lifetime of FRET couples refers to the distance and interaction strength of each interacting pair of molecules. The box plots indicate median results of at least 22 analyzed specks from three independent experiments (*E*). Statistical significance was determined by one-way analysis of variance followed by Tukey's multiple comparisons test. ****, $p < 0.0001$; *n.s.*, not significant. Standard errors of the mean are indicated. *AUC*, area under the curve.

the cytosol. To our initial surprise, 2.1% of macrophages exhibiting two or more specks started to proliferate, subsequently scattering their specks on daughter cells (Fig. 4 and supplemental Movies 2–5, data from two independent experiments).

Discussion

Previous reports directly linked pyroptosis to speck formation and IL-1β release. The question of whether ASC pyroptosomes and ASC-dependent inflammasomes (such as absent in melanoma 2 (AIM2), human NLRP1, and NLRP3 (30)) are two different phenomena, however, remained unanswered. Although some authors detected IL-1β release independent from pyroptosis (31) or pyroptosis without IL-1β release (32), others saw pyroptosis as the result of variable inflammasome activation (20, 33). A third hypothesis claims an all-or-nothing-mechanism with two states: no inflammation or pro-inflammatory cell death/pyroptosis (34). Last, a dual function of caspase-1 was suggested, controlling cell death and autoprocessing with pro-IL-1β cleavage through two different pathways (35), and ASC speck formation was found to be essential for release of mature IL-1β but not for induction of pyroptosis (36). Consequently, the ASC speck is sometimes referred to as an inflammasome and sometimes as a pyroptosome. In this study, we extend current concepts observing *dynamic* changes in iBMDM$^{casp1/11\text{-}ko}$ prior to IL-1β cleavage and release. In our system of Ch-WT cells, mature IL-1β release only occurred with preceding speck formation, and every cell harboring a speck underwent pyroptosis. Thus, we conclude that NLRP3 inflammasome and pyroptosome formation describe the same phenomenon. Consistent with previous reports, we show that speck formation is not disturbed by abrogated enzymatic activity of caspase-1 (27) but, conversely, even supported by it. In response to inflammasome activation, we detected significantly increased numbers of specks in Ch-C284A macrophages (carrying variant p.C284A caspase-1) compared with Ch-WT cells, which led us to three hypotheses: Ch-C284A cells have a lower

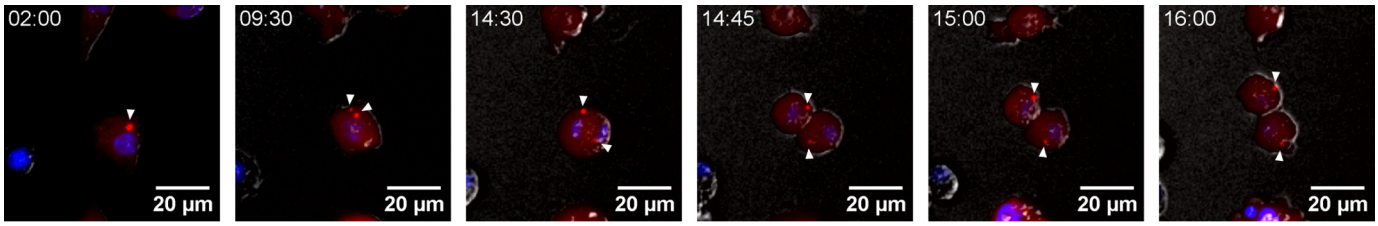

FIGURE 4. **Pyroptosomes of mutant caspase-1 spread during cell division.** iBMDM$^{casp1/11\text{-}ko}$ cells expressed both GFP-ASC and Ch-C284A. Pyroptosome formation was induced by priming with LPS (3 μg/ml) for 5 h and addition of nigericin (10 μM) for 1 h. Cherry channels (*red*) were merged with Hoechst (*blue*) and bright-field (*gray*) channels. Representative images from a time frame between 2 and 16 h after the addition of nigericin are provided. *Arrowheads* indicate a speck that divides into two (at 9:30) prior to cell division (starting at 14:30). The entire movie and further examples can be obtained in the supplemental material.

threshold for the initiation of speck formation; Ch-C284A cells are more resistant to cell death, thus enabling the speck to grow to its full size, hence becoming more easy to detect; and a fraction of specks in Ch-WT cells had already faded after pyroptosis before they were spotted under the microscope. At this point, we can exclude the latter hypothesis as unlikely because the outcomes did not change considerably, minimizing the interval to data acquisition to 5 min, and although the specks faded soon after formation, they never completely vanished. The second hypothesis supports the notion that caspase-1 autoprocessing and the initiation of cell death are two distinct pathways (35, 36). If both effects occur simultaneously rather than subsequently, then a subset of cells may undergo pyroptosis prior to complete inflammasome speck formation. Consistent with that assumption, inflammasome formation in Ch-C284A cells required 20 min until speck intensities had reached their maximum, whereas pyroptosis in Ch-WT cells only took about 5 min. Hence, pyroptotic cell death acts antagonistically to inflammasome speck formation. This may explain the increased speck size and amount of FRET couples we detected in Ch-C284A cells.

In addition, disturbed autoprocessing of variant p.C284A procaspase-1 may play an important role in the stabilization of the pyroptosomes. Here we demonstrate for the first time that ASC speck size and fluorescence intensity over time increase in stimulated Ch-WT cells treated with Ac-YVAD-CMK, whereas caspase-1 enzyme activity, but not the rate of cell death, was affected. Decreased or abrogated autoprocessing of procaspase-1 within the pyroptosome causes more unprocessed procaspase-1 molecules containing CARD domains. Hence, CARD-CARD interactions between procaspase-1 and ASC may be enhanced, thus stabilizing the pyroptosome. Enhanced interaction between caspase-1 and ASC in cells carrying Ch-C284A compared with Ch-WT cells, which we determined through co-immunoprecipitation and FLIM-FRET, supports this hypothesis. Previously, a similar mechanism was suggested for the interaction between procaspase-1 and RIP2 (14).

Of note, speck diameters did not only differ between WT and variant p.C284A caspase-1 but also between caspase-1 and ASC, supporting recent assumptions that the inflammasome is formed by a core of ASC filaments that subsequently recruit procaspase-1 molecules in the periphery (30, 37). However, Man *et al.* (28) recently postulated that ASC molecules may enclose procaspase-1. Taking a closer look at the research of these authors, alternative and not comparable staining techniques were used: a fluorochrome inhibitor of caspases for caspase-1 and antibody staining for ASC. Thus, it should be considered that, because of large antibody size, signals may have not entered the core of the multimeric complex (pyroptosome).

We document for the first time that cells with variant p.C284A caspase-1 form large specks that subsequently spread during cell division. Furthermore, cells remained viable and did not undergo inflammatory cell death. Our findings suggest an association between the pyroptosome and the cell cycle machinery. Indeed, ASC localizes to the nucleus in resting cells and oligomerizes in the perinuclear region in response to activation (19, 38). Furthermore, several reports linked ASC and caspase-1 to the cytoskeleton, including actin and microtubules (39–42).

Regardless of all new insights, this study may be limited by its *in vitro* character. Observations were made in immortalized cell lines that may not entirely resemble the *in vivo* situation. Furthermore, we exclusively focused on caspase-1, excluding potential effects of caspase-11 (corresponding to caspase-4 and -5 in humans). Previously, caspase-11 even more than caspase-1 has been suggested as a driving factor of pyroptotic cell death (9). Thus, it appears likely that macrophages expressing caspase-11 react more vulnerable to pro-inflammatory stimuli compared with the caspase-1- and caspase-11-deficient cells used here. Furthermore, most of the naturally occurring caspase-1 variants other than p.C284A retain some enzymatic activity and warrant further research (12). Treatment with Ac-YVAD-CMK, inhibiting caspase-1 enzymatic activity, did not protect from inflammatory cell death and may therefore reproduce the *in vivo* situation more appropriately. Under these experimental conditions, ASC and caspase-1 specks remained stable even after the decomposition of cells. Pyroptosomes released into the extracellular space are known to act as danger signals because they are internalized by other macrophages augmenting inflammatory responses (22, 23). So, signal amplification through larger extracellular pyroptosomes in patients harboring enzymatically inactive caspase-1 variants is a potential mechanism leading to an inflammatory phenotype.

Through different experimental approaches, we demonstrate that enzymatically inactive caspase-1 stabilizes the ASC pyroptosome both in the intra- and extracellular compartment. Further research is warranted to elucidate which IL-1β independent pathways and cytokines are required downstream of the ASC pyroptosome to evoke autoinflammatory symptoms and whether inflammasome amplification through cell division plays a significant role *in vivo*. Of note, ASC itself has been

reported to be involved in alternative pro-inflammatory pathways in several diseases apart from canonical IL-1β activation (41, 44–47). Numerous pro-inflammatory proteins, including PYPAF1, PYPAF5, PYPAF7, and pyrin, may interact with ASC or procaspase-1 either through their CARD or pyrin domain (48–51). In support of this hypothesis, procaspase-1 variants with disturbed enzymatic activity have been shown to enhance RIP2-mediated NF-κB responses in HEK293T cells (14). Caspase-1/RIP2 interactions, however, have been suggested to occur prior to inflammasome assembly (51).

Proliferation of macrophages *in situ* in response to infection is a recently established and commonly accepted concept (52, 53). Macrophages contribute to pro-inflammatory responses through altering their phenotype in response to the microenvironment, indicating high plasticity (52). Defective macrophage activation may lead to incomplete pathogen elimination and infection. Excessive macrophage activation, on the other hand, may result in inflammatory conditions and tissue damage. Thus, pro-inflammatory signal transduction through propagation of specks during cell division may be a highly efficient and previously not appreciated mechanism during (auto)inflammation. Additionally, macrophages expressing variant p.C284A procaspase-1 resist cell death and therefore may cause an initially weaker but altogether more persistent inflammatory stimulus that may cumulatively be stronger than rapidly occurring pyroptotic cell death of WT cells.

In conclusion, mutant caspase-1 exerts stabilizing effects on the ASC pyroptosome both in the intra- and extracellular compartment. Pyroptosome spreading through cell division is a new concept of innate immune response amplification, potentially contributing to systemic inflammation in patients with naturally occurring caspase-1 variants. The involvement of our observations in the exact molecular pathophysiology of interleukin 1-converting enzyme fever and other inflammatory diseases is the subject of ongoing research that will contribute to the development of novel disease biomarkers and therapeutic targets.

Experimental Procedures

Plasmids—Murine ASC and wild-type caspase-1 were obtained from immortalized bone marrow-derived macrophages by RNA isolation and cDNA synthesis using the RNeasy Mini Kit (Qiagen, Germantown, MD) and SuperScript® II reverse transcriptase (Thermo Fisher Scientific, Schwerte, Germany). The p.C284A variant was generated by site-directed mutagenesis (Stratagene, La Jolla, CA) following standard protocols. cDNA fragments were cloned into the lentiviral transfer vector p6NST51 and fused to mCherry at their N terminus (p6NST51.mCherry.CASP1) or into the lentiviral transfer vector p6NST53 and then fused to EGFP at their N terminus (p6NST53.EGFP.ASC). All constructs underwent quality control by restriction enzyme digestion and Sanger sequencing. Both the p6NST51 and p6NST53 vectors were kindly provided by Prof. Dirk Lindemann (Institute of Virology, University Hospital Carl Gustav Carus, Technische Universität Dresden, Germany). The two plasmids applied here only differed in their resistance for eukaryotic selection. mCherry and EGFP plasmids were purchased from Clontech (Mountain View, CA).

Cell Culture—Murine immortalized bone marrow derived caspase-1/-11 knock-out macrophages (iBMDM$^{casp1/11\text{-}ko}$) were kindly provided by Prof. Veit Hornung (Munich, Germany). Briefly, this cell line was generated by J2 immortalization of BMDMs from a strain 129 background (43, 54). To produce lentiviral vector particles, HEK293T cells were transfected with lentiviral transfer plasmids in combination with the plasmids psPAX2 and pMD2.G. iBMDMs were transduced with a multiplicity of infection of 0.1 (p6NST51.mCherry.CASP1) or 0.2 (p6NST53.EGFP.ASC) and selected with zeocin or G418, respectively. Cells were maintained in 5% CO_2 at 37 °C in Iscove's basal medium supplemented with 10% fetal calf serum, 2 mM L-glutamine, and antibiotics.

Antibodies and Reagents—The following antibodies were used: anti-procaspase-1 M-20 (p10 subunit, sc-514) from Santa Cruz Biotechnology (Santa Cruz, CA), anti-procaspase-1 (p20 subunit, Casper-1, AG-20B-0042) from Adipogen (San Diego, CA), anti-IL-1β (recognizing pro- and mature forms, AF-401-NA) from R&D Systems (Minneapolis, MN), anti-ASC (AL177) from Adipogen, anti-α-tubulin DM1A (T9026) from Sigma-Aldrich (St. Louis, MO), anti-β-actin (clone AC-74, A5316) from Sigma-Aldrich, HRP-linked anti-rabbit (NA9340) from GE Healthcare, HRP-linked anti-mouse (P0260) and HRP-linked anti-goat (P0449) from DakoCytomation (Glostrup, Denmark), and Alexa Fluor 488-linked anti-rabbit (A-11008) from Life Technologies. Nigericin and ultrapure LPS from *Escherichia coli* O111:B4 were obtained from InvivoGen (Toulouse, France). Ac-YVAD-CMK was purchased from Enzo Life Sciences (Farmingdale, NY) and diluted in CryoSure DMSO (Sigma-Aldrich). Nuclei in live cell imaging experiments were stained with Nuc Blue® Live ReadyProbes® reagent (Thermo Fisher Scientific).

Co-Immunoprecipitation—iBMDMcasp$^{1/11\text{-}ko}$ were primed, stimulated as indicated, and lysed with Pierce Direct IP lysis/wash buffer containing 0.025 M Tris, 0.15 M NaCl, 0.001 M EDTA, 1% Nonidet P-40, and 5% glycerol (pH 7.4) (Pierce® Direct IP Kit, Thermo Scientific). Determined amounts of clarified lysates were incubated with Pierce control agarose resin (cross-linked 4% beaded agarose) to ensure the absence of non-specific binding before the incubation with AminoLink® Plus coupling resin (both Pierce Direct IP Kit, Thermo Scientific) coupled with anti-ASC (AL-177, Adipogen) overnight at 4 °C with rotation. Precipitates were analyzed by SDS-PAGE and Western blotting. Densitometric analysis was performed using ImageJ (http://imagej.nih.gov/ij/).

Protein Expression Analysis—Protein expression was determined in serum-free cell supernatants or cell lysates by SDS-PAGE using caspase-1 polyclonal antibody (sc-514, Santa Cruz Biotechnology) and IL-1β polyclonal antibody (AF-401-NA, R&D Systems). Cells were lysed and processed as reported previously (14, 51). Concentrations of mature IL-1β in the supernatant were determined by cytometric bead arrays from BD Biosciences.

Assessment of Cell Death—Lactate dehydrogenase release into the supernatant was determined with the Cytotoxicity Detection Kit PLUS (Roche Applied Science) following the instructions of the manufacturer.

Immunofluorescence Staining—iBMDM$^{casp1/11\text{-}ko}$ were primed, stimulated as indicated, fixed in 4% paraformaldehyde (Sigma-Aldrich) for 15 min at room temperature, washed, and permeabilized in PBS containing 0.04% saponin (Sigma-Aldrich) and 1% BSA (Sigma-Aldrich) for 1 h. Then cells were stained with the appropriate primary antibody for 1 h, followed by staining with the secondary antibody for 45 min. Coverslips were mounted on glass slides in Vectashield mounting medium (Vector Laboratories, Burlingame, CA).

Confocal and Fluorescence Microscopy—Live cell imaging was conducted in Iscove's modified Dulbecco's medium (Thermo Fisher Scientific/GIBCO) at 37 °C and 5% CO_2 at the light microscopy facility of the Biotechnology Center of the Technical University Dresden and the Center for Regenerative Therapies. Confocal laser scanning was performed on an inverted Leica TCS SP5 microscope (Leica Microsystems, Wetzlar, Germany) using a Leica HC PL APO ×20/0.7 NA immersion objective and a Leica HC PL APO ×63/1.4–0.6 NA oil objective. Images were acquired and processed with LAS AF software using 405-, 488-, and 561-nm laser lines for excitation and spectral detection bands of 410–493, 498–552, and 571–740 nm.

Long-term live cell imaging (over 3 or 17 h) was conducted with a Zeiss Axiovert 200 M microscope (Carl Zeiss Microscopy GmbH) using a Zeiss Plan-Apochromat ×10/0.45 NA objective and reflectors for Hoechst staining (EX, 340–380 nm; EM, 435–485 nm), GFP (EX, 465–495 nm; EM, 500–540 nm), and cherry (EX, 530–560 nm; EM, 590–650 nm). A charge-coupled device Coolsnap HQ camera (Photometrics) and MetaMorph (Visitron Systems GmbH, Puchheim, Germany) software were used for data acquisition.

Imaging of fixed cells was performed with a Zeiss Axiovert 200 M microscope using a Zeiss Achroplan ×100/1.25 NA oil objective and a Zeiss Plan-Neofluar ×10/0.3 NA objective as well as filter sets for DAPI staining (EX, 365 nm; EM, 420–470 nm), GFP (EX, 450–490 nm; EM, 500–550 nm), and cherry (EX, 537.5–562.5 nm; EM, 570–640 nm). For image acquisition, a Zeiss Axiocam MRm camera and Axiovision software (Carl Zeiss Microscopy GmbH) were used.

Image Processing—Image processing was carried out with ImageJ/Fiji software. Pyroptosomes were counted manually in the mCherry or GFP channel, and total cell numbers were determined by quantification of nuclei in the Hoechst channel. Pyroptosome intensity was measured as the maximum intensity of each speck after normalization for background signals. For analysis of the pyroptosome diameter, the full width at half-maximum intensity was applied.

FLIM-FRET—iBMDM$^{casp1/11\text{-}ko}$ were transduced and stimulated as indicated in the figure legends. Prior to FLIM, cells were fixed in 4% paraformaldehyde for 15 min at room temperature, washed, and covered with PBS. Time-correlated single photon counting was performed at the light microscopy facility of the Biotechnology Center of the Technical University Dresden and the Center for Regenerative Therapies on a confocal laser-scanning microscope (Zeiss LSM780, Carl Zeiss Microsopy GmbH, Germany) equipped with a time-correlated single photon counting set (Becker & Hickl GmbH, Berlin, Germany) using a Zeiss C-Apochromat ×40/1.20 NA water objective. Excitation of the donor EGFP was performed with a 473-nm diode laser pulsed at 50 MHz and 0.8% laser power. For detection, a band-pass filter (500–550 nm) and hybrid photomultiplier tube detectors were used. Confocal imaging was performed in ZEN using a C-Apochromat ×40/1.20 NA water objective, 473- and 561-nm laser lines for EGFP and mCherry, respectively, and photomultiplier tube detectors with detection bands of 482–556 and 580–711 nm. Fluorescence lifetimes were calculated for the brightest pixel within each speck with SPCImage software. Approximately 2000 photons were acquired for the brightest pixel, and photon statistics were further improved by 5 × 5 pixel binning. Data were tail-fitted to single-exponential decay and further refined by a double-exponential decay model, $f(t) = A_1\exp(-t/\tau_1) + A_2\exp(-t/\tau_2)$, using fixed lifetime donor values (τ_2). τ stands for the fluorescence lifetime of the exponential component and A for the amplitude (or fraction) of individual contribution. The applied model allows resolving both fluorescence lifetime and fractional contribution of interacting and non-interacting donor molecules. Goodness of fit was assessed by calculated standard least squares (χ^2).

Statistics—Statistical analysis was performed using GraphPad Prism software. Statistical significance of FLIM-FRET experiments was determined by one-way analysis of variance followed by Tukey's multiple comparisons test. All other results were evaluated using Mann-Whitney test. *, $p < 0.05$; **, $p < 0.01$; ***, $p < 0.001$; ****, $p < 0.0001$; n.s., not significant. Standard errors of the mean are indicated.

Author Contributions—R. S. conducted most of the experiments, analyzed the data, and wrote most of the paper. F. K. contributed to the live cell imaging experiments, generated virally transduced cell lines, and performed co-immunoprecipitation experiments. M. C. H. conducted experiments on the impact of fluorescent tags on procaspase-1 and helped with designing the study. S. R. conducted experiments on the IL-1β secretion of cells and constructed plasmids for expression of fluorescently labeled proteins. W. S. performed the FLIM-FRET experiments and analyzed the data. C. M. H. and A. R. W. contributed to the interpretation of data and revised the manuscript. S. R. H. designed the study, conducted *in vivo* live cell imaging experiments, and wrote the paper with R. S. All authors reviewed the results and approved the final version of the manuscript.

Acknowledgments—Images were generated at the Biopolis Dresden Imaging Platform (BioDIP), including the Biotechnology Center of the Technical University Dresden (BIOTEC) and the Center for Regenerative Therapies (CRTD). We thank the light microscopy facility of the CRTD/BIOTEC, especially Hella Hartmann and Markus Burkhardt, for excellent support. We thank Prof. Dirk Lindemann (Dresden, Germany) for kindly providing plasmids. We also thank Prof. Veit Hornung (Munich, Germany) for the murine immortalized bone marrow derived caspase-1/11 knockout macrophages (iBMDM$^{casp1/11\text{-}ko}$).

References

1. Martinon, F., Burns, K., and Tschopp, J. (2002) The inflammasome: a molecular platform triggering activation of inflammatory caspases and processing of proIL-β. *Mol. Cell* **10,** 417–426
2. Heymann, M. C., and Hofmann, S. R. (2011) Novel inflammasomes and type II diabetes, intestinal inflammation and psoriasis as newly inflam-

masome-related diseases. *J. Genet. Syndr. Gene Ther.* **S3:001,** 1–8
3. Jiménez Fernández, D., and Lamkanfi, M. (2015) Inflammatory caspases: key regulators of inflammation and cell death. *Biol. Chem.* **396,** 193–203
4. Yamin, T. T., Ayala, J. M., and Miller, D. K. (1996) Activation of the native 45-kDa precursor form of interleukin-1-converting enzyme. *J. Biol. Chem.* **271,** 13273–13282
5. Wilson, K. P., Black, J. A., Thomson, J. A., Kim, E. E., Griffith, J. P., Navia, M. A., Murcko, M. A., Chambers, S. P., Aldape, R. A., and Raybuck, S. A. (1994) Structure and mechanism of interleukin-1 β converting enzyme. *Nature* **370,** 270–275
6. Rühl, S., and Broz, P. (2015) Caspase-11 activates a canonical NLRP3 inflammasome by promoting K^+ efflux. *Eur. J. Immunol.* **45,** 2927–2936
7. Bergsbaken, T., Fink, S. L., and Cookson, B. T. (2009) Pyroptosis: host cell death and inflammation. *Nat. Rev. Microbiol.* **7,** 99–109
8. Broz, P. (2015) Immunology: caspase target drives pyroptosis. *Nature* **526,** 642–643
9. Kayagaki, N., Warming, S., Lamkanfi, M., Vande Walle, L., Louie, S., Dong, J., Newton, K., Qu, Y., Liu, J., Heldens, S., Zhang, J., Lee, W. P., Roose-Girma, M., and Dixit, V. M. (2011) Non-canonical inflammasome activation targets caspase-11. *Nature* **479,** 117–121
10. Kayagaki, N., Stowe, I. B., Lee, B. L., O'Rourke, K., Anderson, K., Warming, S., Cuellar, T., Haley, B., Roose-Girma, M., Phung, Q. T., Liu, P. S., Lill, J. R., Li, H., Wu, J., Kummerfeld, S., *et al.* (2015) Caspase-11 cleaves gasdermin D for non-canonical inflammasome signaling. *Nature* **526,** 666–671
11. Shi, J., Zhao, Y., Wang, K., Shi, X., Wang, Y., Huang, H., Zhuang, Y., Cai, T., Wang, F., and Shao, F. (2015) Cleavage of GSDMD by inflammatory caspases determines pyroptotic cell death. *Nature* **526,** 660–665
12. Luksch, H., Romanowski, M. J., Chara, O., Tüngler, V., Caffarena, E. R., Heymann, M. C., Lohse, P., Aksentijevich, I., Remmers, E. F., Flecks, S., Quoos, N., Gramatté, J., Petzold, C., Hofmann, S. R., Winkler, S., *et al.* (2013) Naturally occurring genetic variants of human caspase-1 differ considerably in structure and the ability to activate interleukin-1β. *Hum. Mutat.* **34,** 122–131
13. Luksch, H., Winkler, S., Heymann, M. C., Schulze, F., Hofmann, S. R., Roesler, J., and Rösen-Wolff, A. (2015) Current knowledge on procaspase-1 variants with reduced or abrogated enzymatic activity in autoinflammatory disease. *Curr. Rheumatol. Rep.* **17,** 45
14. Heymann, M. C., Winkler, S., Luksch, H., Flecks, S., Franke, M., Ruß, S., Ozen, S., Yilmaz, E., Klein, C., Kallinich, T., Lindemann, D., Brenner, S., Ganser, G., Roesler, J., Rösen-Wolff, A., and Hofmann, S. R. (2014) Human procaspase-1 variants with decreased enzymatic activity are associated with febrile episodes and may contribute to inflammation via RIP2 and NF-κB signaling. *J. Immunol.* **192,** 4379–4385
15. Elliott, E. I., and Sutterwala, F. S. (2015) Initiation and perpetuation of NLRP3 inflammasome activation and assembly. *Immunol. Rev.* **265,** 35–52
16. Sharma, D., and Kanneganti, T. D. (2016) The cell biology of inflammasomes: mechanisms of inflammasome activation and regulation. *J. Cell Biol.* **213,** 617–629
17. Broz, P., and Dixit, V. M. (2016) Inflammasomes: mechanism of assembly, regulation and signalling. *Nat. Rev. Immunol.* **16,** 407–420
18. Broz, P. (2016) Inflammasomes: Intracellular detection of extracellular bacteria. *Cell Res.* 10.1038/cr.2016.67
19. Bryan, N. B., Dorfleutner, A., Rojanasakul, Y., and Stehlik, C. (2009) Activation of inflammasomes requires intracellular redistribution of the apoptotic speck-like protein containing a caspase recruitment domain. *J. Immunol.* **182,** 3173–3182
20. Lu, A., Magupalli, V. G., Ruan, J., Yin, Q., Atianand, M. K., Vos, M. R., Schröder, G. F., Fitzgerald, K. A., Wu, H., and Egelman, E. H. (2014) Unified polymerization mechanism for the assembly of ASC-dependent inflammasomes. *Cell* **156,** 1193–1206
21. Kersse, K., Lamkanfi, M., Bertrand, M. J., Vanden Berghe, T., and Vandenabeele, P. (2011) Interaction patches of procaspase-1 caspase recruitment domains (CARDs) are differently involved in procaspase-1 activation and receptor-interacting protein 2 (RIP2)-dependent nuclear factor κB signaling. *J. Biol. Chem.* **286,** 35874–35882
22. Baroja-Mazo, A., Martín-Sánchez, F., Gomez, A. I., Martínez, C. M., Amores-Iniesta, J., Compan, V., Barberà-Cremades, M., Yagüe, J., Ruiz-Ortiz, E., Antón, J., Buján, S., Couillin, I., Brough, D., Arostegui, J. I., and Pelegrín, P. (2014) The NLRP3 inflammasome is released as a particulate danger signal that amplifies the inflammatory response. *Nat. Immunol.* **15,** 738–748
23. Franklin, B. S., Bossaller, L., De Nardo, D., Ratter, J. M., Stutz, A., Engels, G., Brenker, C., Nordhoff, M., Mirandola, S. R., Al-Amoudi, A., Mangan, M. S., Zimmer, S., Monks, B. G., Fricke, M., Schmidt, R. E., *et al.* (2014) The adaptor ASC has extracellular and "prionoid" activities that propagate inflammation. *Nat. Immunol.* **15,** 727–737
24. Bauernfeind, F. G., Horvath, G., Stutz, A., Alnemri, E. S., MacDonald, K., Speert, D., Fernandes-Alnemri, T., Wu, J., Monks, B. G., Fitzgerald, K. A., Hornung, V., and Latz, E. (2009) Cutting edge: NF-κB activating pattern recognition and cytokine receptors license NLRP3 inflammasome activation by regulating NLRP3 expression. *J. Immunol.* **183,** 787–791
25. Mariathasan, S., Weiss, D. S., Newton, K., McBride, J., O'Rourke, K., Roose-Girma, M., Lee, W. P., Weinrauch, Y., Monack, D. M., and Dixit, V. M. (2006) Cryopyrin activates the inflammasome in response to toxins and ATP. *Nature* **440,** 228–232
26. Heymann, M. C., Rabe, S., Ruβ, S., Kapplusch, F., Schulze, F., Stein, R., Winkler, S., Hedrich, C. M., Rösen-Wolff, A., and Hofmann, S. R. (2015) Fluorescent tags influence the enzymatic activity and subcellular localization of procaspase-1. *Clin. Immunol.* **160,** 172–179
27. Fernandes-Alnemri, T., Wu, J., Yu, J.-W., Datta, P., Miller, B., Jankowski, W., Rosenberg, S., Zhang, J., and Alnemri, E. S. (2007) The pyroptosome: a supramolecular assembly of ASC dimers mediating inflammatory cell death via caspase-1 activation. *Cell Death Differ.* **14,** 1590–1604
28. Man, S. M., Hopkins, L. J., Nugent, E., Cox, S., Glück, I. M., Tourlomousis, P., Wright, J. A., Cicuta, P., Monie, T. P., and Bryant, C. E. (2014) Inflammasome activation causes dual recruitment of NLRC4 and NLRP3 to the same macromolecular complex. *Proc. Natl. Acad. Sci. U.S.A.* **111,** 7403–7408
29. Lakowicz, J. R. (2010) Principles of fluorescence spectroscopy. pp 367–394, Springer, New York, NY
30. Lu, A., and Wu, H. (2015) Structural mechanisms of inflammasome assembly. *FEBS J.* **282,** 435–444
31. Stoffels, M., Zaal, R., Kok, N., van der Meer, J. W., Dinarello, C. A., and Simon, A. (2015) ATP-induced IL-1β specific secretion: true under stringent conditions. *Front. Immunol.* **6,** 54
32. Aachoui, Y., Sagulenko, V., Miao, E. A., and Stacey, K. J. (2013) Inflammasome-mediated pyroptotic and apoptotic cell death, and defense against infection. *Curr. Opin. Microbiol.* **16,** 319–326
33. Latz, E., Xiao, T. S., and Stutz, A. (2013) Activation and regulation of the inflammasomes. *Nat. Rev. Immunol.* **13,** 397–411
34. Liu, T., Yamaguchi, Y., Shirasaki, Y., Shikada, K., Yamagishi, M., Hoshino, K., Kaisho, T., Takemoto, K., Suzuki, T., Kuranaga, E., Ohara, O., and Miura, M. (2014) Single-cell imaging of caspase-1 dynamics reveals an all-or-none inflammasome signaling response. *Cell Rep.* **8,** 974–982
35. Broz, P., von Moltke, J., Jones, J. W., Vance, R. E., and Monack, D. M. (2010) Differential requirement for Caspase-1 autoproteolysis in pathogen-induced cell death and cytokine processing. *Cell Host Microbe* **8,** 471–483
36. Dick, M. S., Sborgi, L., Rühl, S., Hiller, S., and Broz, P. (2016) ASC filament formation serves as a signal amplification mechanism for inflammasomes. *Nat. Commun.* **7,** 11929
37. Hauenstein, A. V., Zhang, L., and Wu, H. (2015) The hierarchical structural architecture of inflammasomes, supramolecular inflammatory machines. *Curr. Opin. Struct. Biol.* **31,** 75–83
38. Martin, B. N., Wang, C., Willette-Brown, J., Herjan, T., Gulen, M. F., Zhou, H., Bulek, K., Franchi, L., Sato, T., Alnemri, E. S., Narla, G., Zhong, X.-P., Thomas, J., Klinman, D., Fitzgerald, K. A., *et al.* (2014) IKKα negatively regulates ASC-dependent inflammasome activation. *Nat. Commun.* **5,** 4977
39. Kayalar, C., Ord, T., Testa, M. P., Zhong, L. T., and Bredesen, D. E. (1996) Cleavage of actin by interleukin 1 β-converting enzyme to reverse DNase I inhibition. *Proc. Natl. Acad. Sci. U.S.A.* **93,** 2234–2238
40. Li, J., Yin, H. L., and Yuan, J. (2008) Flightless-I regulates proinflammatory caspases by selectively modulating intracellular localization and caspase activity. *J. Cell Biol.* **181,** 321–333

41. Ippagunta, S. K., Malireddi, R. K., Shaw, P. J., Neale, G. A., Vande Walle, L., Green, D. R., Fukui, Y., Lamkanfi, M., and Kanneganti, T.-D. (2011) The inflammasome adaptor ASC regulates the function of adaptive immune cells by controlling Dock2-mediated Rac activation and actin polymerization. *Nat. Immunol.* **12,** 1010–1016
42. Misawa, T., Takahama, M., Kozaki, T., Lee, H., Zou, J., Saitoh, T., and Akira, S. (2013) Microtubule-driven spatial arrangement of mitochondria promotes activation of the NLRP3 inflammasome. *Nat. Immunol.* **14,** 454–460
43. Blasi, E., Radzioch, D., Durum, S. K., and Varesio, L. (1987) A murine macrophage cell line, immortalized by v-raf and v-myc oncogenes, exhibits normal macrophage functions. *Eur. J. Immunol.* **17,** 1491–1498
44. Abdelaziz, D. H., Gavrilin, M. A., Akhter, A., Caution, K., Kotrange, S., Khweek, A. A., Abdulrahman, B. A., Hassan, Z. A., El-Sharkawi, F. Z., Bedi, S. S., Ladner, K., Gonzalez-Mejia, M. E., Doseff, A. I., Mostafa, M., Kanneganti, T.-D., *et al.* (2011) ASC-dependent and independent mechanisms contribute to restriction of *Legionella pneumophila* infection in murine macrophages. *Front. Microbiol.* **2,** 18
45. Taxman, D. J., Holley-Guthrie, E. A., Huang, M. T., Moore, C. B., Bergstralh, D. T., Allen, I. C., Lei, Y., Gris, D., and Ting, J. P. (2011) The NLR adaptor ASC/PYCARD regulates DUSP10, mitogen-activated protein kinase (MAPK), and chemokine induction independent of the inflammasome. *J. Biol. Chem.* **286,** 19605–19616
46. Taxman, D. J., Zhang, J., Champagne, C., Bergstralh, D. T., Iocca, H. A., Lich, J. D., and Ting, J. P. (2006) Cutting edge: ASC mediates the induction of multiple cytokines by *Porphyromonas gingivalis* via caspase-1-dependent and -independent pathways. *J. Immunol.* **177,** 4252–4256
47. Kolly, L., Karababa, M., Joosten, L. A., Narayan, S., Salvi, R., Pétrilli, V., Tschopp, J., van den Berg, W. B., So, A. K., and Busso, N. (2009) Inflammatory role of ASC in antigen-induced arthritis is independent of caspase-1, NALP-3, and IPAF. *J. Immunol.* **183,** 4003–4012
48. Manji, G. A., Wang, L., Geddes, B. J., Brown, M., Merriam, S., Al-Garawi, A., Mak, S., Lora, J. M., Briskin, M., Jurman, M., Cao, J., DiStefano, P. S., and Bertin, J. (2002) PYPAF1, a PYRIN-containing Apaf1-like protein that assembles with ASC and regulates activation of NF-κB. *J. Biol. Chem.* **277,** 11570–11575
49. Grenier, J. M., Wang, L., Manji, G. A., Huang, W.-J., Al-Garawi, A., Kelly, R., Carlson, A., Merriam, S., Lora, J. M., Briskin, M., DiStefano, P. S., and Bertin, J. (2002) Functional screening of five PYPAF family members identifies PYPAF5 as a novel regulator of NF-κB and caspase-1. *FEBS Lett.* **530,** 73–78
50. Wang, L., Manji, G. A., Grenier, J. M., Al-Garawi, A., Merriam, S., Lora, J. M., Geddes, B. J., Briskin, M., DiStefano, P. S., and Bertin, J. (2002) PYPAF7, a novel PYRIN-containing Apaf1-like protein that regulates activation of NF-κB and caspase-1-dependent cytokine processing. *J. Biol. Chem.* **277,** 29874–29880
51. Sarkar, A., Duncan, M., Hart, J., Hertlein, E., Guttridge, D. C., and Wewers, M. D. (2006) ASC directs NF-κB activation by regulating receptor interacting protein-2 (RIP2) caspase-1 interactions. *J. Immunol.* **176,** 4979–4986
52. Zhang, L., and Wang, C.-C. (2014) Inflammatory response of macrophages in infection. *Hepatobiliary & Pancreatic Diseases International* **13,** 138–152
53. Gentek, R., Molawi, K., and Sieweke, M. H. (2014) Tissue macrophage identity and self-renewal. *Immunol. Rev.* **262,** 56–73
54. Blasi, E., Mathieson, B. J., Varesio, L., Cleveland, J. L., Borchert, P. A., and Rapp, U. R. (1985) Selective immortalization of murine macrophages from fresh bone marrow by a raf/myc recombinant murine retrovirus. *Nature* **318,** 667–670